Geomechanics and Engineering, *Vol. 18, No. 3 (2019) 315-328*
DOI: https://doi.org/10.12989/gae.2019.18.3.315

Small- and large-scale analysis of bearing capacity and load-settlement behavior of rock-soil slopes reinforced with geogrid-box method

Gholam Moradi[1a], Arvin Abdolmaleki[1b] and Parham Soltani*[2]

[1]*Faculty of Civil Engineering, University of Tabriz, Tabriz, Iran*
[2]*Department of Textile Engineering, Isfahan University of Technology, Isfahan 84156-83111, Iran*

(Received October 30, 2018, Revised June 4, 2019, Accepted June 7, 2019)

Abstract. This paper presents an investigation on bearing capacity, load-settlement behavior and safety factor of rock-soil slopes reinforced using geogrid-box method (GBM). To this end, small-scale laboratory studies were carried out to study the load-settlement response of a circular footing resting on unreinforced and reinforced rock-soil slopes. Several parameters including unit weight of rock-soil materials (loose- and dense-packing modes), slope height, location of footing relative to the slope crest, and geogrid tensile strength were studied. A series of finite element analysis were conducted using ABAQUS software to predict the bearing capacity behavior of slopes. Limit equilibrium and finite element analysis were also performed using commercially available software SLIDE and ABAQUS, respectively to calculate the safety factor.

It was found that stabilization of rock-soil slopes using GBM significantly improves the bearing capacity and settlement behavior of slopes. It was established that, the displacement contours in the dense-packing mode distribute in a broader and deeper area as compared with the loose-packing mode, which results in higher ultimate bearing load. Moreover, it was found that in the loose-packing mode an increase in the vertical pressure load is accompanied with an increase in the soil settlement, while in the dense-packing mode the load-settlement curves show a pronounced peak. Comparison of bearing capacity ratios for the dense- and loose-packing modes demonstrated that the maximum benefit of GBM is achieved for rock-soil slopes in loose-packing mode. It was also found that by increasing the slope height, both the initial stiffness and the bearing load decreases. The results indicated a significant increase in the ultimate bearing load as the distance of the footing to the slope crest increases. For all the cases, a good agreement between the laboratory and numerical results was observed.

Keywords: rock-soil slope; geogrid-box method; bearing capacity; safety factor; finite element analysis; limit equilibrium

1. Introduction

Physical or laboratory modeling is widely used in geotechnical practice, mainly to study the bearing capacity behavior of foundations and to validate the analytical and numerical models. In general, laboratory modeling can be carried out through either a large-scale or a small-scale model. Large-scale modeling is generally performed with the real site conditions and is a more accurate one than small-scale modeling. However, large-scale laboratory model tests are hard to operate due to their large sizes and the cost is significantly higher than small-scale tests. Therefore the small-scale tests are carried out extensively as an alternative for large-scale models to deal with such drawbacks. The small-scale tests are appropriate methods to study the effect of variable parameters on the bearing capacity behavior of slopes. However, the results obtained from these tests are related to the size of physical models. These size effects are commonly known as scale effects.

The bearing capacity of the foundations is a primary concern for civil and geotechnical engineers as it helps in the assessment and design of safe foundation systems (Feng *et al*. 2018). Extensive studies have been carried out regarding the effects of scale on bearing capacity and settlement behavior of shallow foundations on low strength soils (Berry 1935, Meyerhof 1963, Kusakabe *et al*. 1991, Zhu *et al*. 2001, Ukritchon *et al*. 2003, Cerato and Lutenegger 2007, Chung and Cascante 2007, Kumar and Khatri 2008, Nareeman 2012, Ashtiani *et al*. 2015, Hou *et al*. 2017, Zhang and Zhou 2018). Berry (1935) investigated the stability of granular mixtures and demonstrated that the bearing capacity of surface model circular footings increased disproportionately with increasing the footing size on dense-packing sand. Meyerhof (1963) study on the scale effects has led to introducing some formula for calculating the bearing capacity of shallow foundations. It was found that the shape factor decreases with the increase in footing size. Kusakabe *et al*. (1991) conducted an experimental study on bearing capacity factor and shape factor for circular and rectangular footings and exhibited a similar effect of footing size on shape factor. It was concluded that shape factor decreases by 33% as the footing size increases from a few centimeters to 3 m. Zhu *et al*. (2001) conducted an experimental and numerical study and investigated the scale effect of the strip and circular footings resting on

*Corresponding author, Ph.D.
E-mail: pa.soltani@cc.iut.ac.ir
[a]Ph.D.
[b]Ph.D. Student

ISSN: 2005-307X (Print), 2092-6219 (Online)

dense-packing sand. It was established that bearing capacity increases exponentially with increasing footing size. Ukritchon, Whittle *et al*. (2003) studied the effect of internal friction angle on the bearing capacity of surface strip footing on a frictional soil and reported a 5 to 30% change in the bearing capacity by increasing internal friction angle from 5 to 45°. Scale effects of shallow foundation bearing capacity rested on granular material was investigated by Cerato and Lutenegger (2007). A reduction in the bearing capacity with increasing the footing width was reported. The effect of the footing width on the bearing capacity by incorporating the variation of soil friction angle with mean principal stress was also studied by Kumar and Khatri (2008). The results indicated a linear relationship on a logarithmic scale for the relationship between the bearing capacity and the foundation width. Nareeman (2012) conducted an investigation of the scale effects on bearing capacity and settlement behavior in adhesive soils. It was found that the bearing capacity shape factor increased slightly with increasing width of the footing. Hou *et al*. (2017) investigated bearing capacity of strip foundations in horizontal-vertical reinforced soils. An analytical solution was presented including the traditional factors of soil, unit soil weight, footing width, number of horizontal-vertical reinforcement layers, and reinforcement geometry. Ahmadi and Moghadam (2017) investigated the effect of geogrid aperture size and soil particle size on geogrid-soil interaction under pull-out loading. It was found that aperture dimension is a profound factor in the pull-out resistance of geogrids and should be selected properly based on the particle size distribution of the soil.

The focus of these studies is mainly on the scale effect of shallow foundations. These researches have investigated the effect of footing size, footing type, footing shape and soil type on bearing capacity. There exist many situations such as power pole footings and footings for bridge abutments resting on sloping embankments, in which due to the non-availability of suitable construction sites, footings are located on/or adjacent to the rock-soil slope. These footings suffer from considerably lower factor of safety and bearing capacity compared to those constructed on the flat ground.

In the last decade, increased infrastructural developments and construction demands in Middle East and elsewhere has necessitated design and construction of reinforced slopes. Currently several techniques are being used for stabilization of slopes including, but not limited to, inclusion of geosynthetic reinforcement layer (Viswanadham and Konig 2009, Turker *et al*. 2014, Touze-Foltz *et al*. 2016), inclusion of grid-anchor (Mosallanezhad *et al*. 2008, Alamshahi and Hataf 2009, Hataf and Sadr 2015, Xu and Yin 2016), pile reinforcement (Ausilio *et al*. 2001, Fahimifar and Soroush 2005, Won *et al*. 2005, Ranjbarnia *et al*. 2015), granular trench (Unnikrishnan and Rajan 2012, Bouassida *et al*. 2014, Abhishek *et al.* 2015, Conte and Troncone 2018) and altering the geometry of slope (Alejano *et al*. 2007, Xiao *et al*. 2010, Puzrin *et al*. 2015). Among these methods, use of geosynthetic reinforcements has revolutionized the field of ground improvement and has gained significant attention in recent years. The studies conducted in this field have established that inclusion of reinforcements can improve both the ultimate bearing capacity and settlement characteristics of the footing.

One of the possible solutions to increase the stability of slope is to reinforce the sloped fill with inclusion of several layers of geogrid, which is known as layered geogrid method (LGM). LGM has been proven as an effective reinforcement measure for unstable slopes. In the last years, numerous studies have been conducted on bearing capacity of the foundations located on the slopes reinforced with LGM (Srbulov 2001, Yoo 2001, El Sawwaf 2007, Alamshahi and Hataf 2009, Naeini *et al*. 2012, Demir, Yildiz *et al*. 2014, Keskin and Laman 2014, Tavakoli *et al*. 2016). The ultimate bearing capacity of strip footings rested on geogrid-reinforced sand slopes was investigated by Keskin and Laman (2014) and the significant positive effect of stabilization on bearing capacity was emphasized. Yoo (2001) conducted a laboratory investigation to evaluate the bearing capacity behavior of strip footing resting on sand slopes reinforced using LGM. The results indicated that the bearing capacity of footing can considerably be improved by inclusion of layers of geogrid and the magnitude of increase is a function of the geogrid distribution. Alamshahi and Hataf (2009) investigated the bearing capacity and load-settlement behavior of strip footing on sand slope stabilized with LGM and grid-anchor. It was established that both the load-settlement behavior and bearing capacity of footing can significantly be improved by the inclusion of a reinforcing layer at the appropriate location in the fill slope. Naeini, Rabe *et al*. (2012) conducted an experimental investigation on bearing capacity and settlement behavior of strip footing resting on clayey slopes reinforced with LGM. The results showed that inclusion of geogrid layer can significantly enhance both the bearing capacity and load-settlement behavior of footing. It was also shown that the bearing capacity increase with the increase in edge distance. Tavakoli *et al*. (2016) conducted an experimental study on the behavior of slope reinforced with LGM with respect to aggregate size. It was found that the particle size has paramount influence on the behavior of reinforced slope and leads to the change in modal behavior at failure state. El Sawwaf (2007) studied the bearing capacity behavior of strip footing resting on a soft clay slopes. To enhance the bearing capacity of the layer, the upper part of the slope was replaced with geogrid-reinforced sand. The results showed that using this method not only results in an improvement in the performance of the footing, but also reduces the sand thickness required to achieve the appropriate settlement.

Although several studies have been conducted on scale effect on bearing capacity behavior of shallow foundations, a limited number of works has been conducted on the bearing capacity and settlement behavior of reinforced slopes based on a scale effect approach. Moreover, most of these researches have been performed on soil slopes, especially those made of sand, while there are some situations such as conglomerate slopes in which the slope consists of soli-rock matrix of fine-grained soil less than 1mm in size to cobbles of about 75 mm in size.

In 2014, the authors (Fahimifar *et al*. 2014) proposed a new method called geogrid-box method (GBM) for the stabilization of rock slopes. GBM is a reinforcement technique through which the geogrid-boxes are filled up with crushed rocks in a way that polymeric mesh elements interlock particles and groups of particles together to form a unitary, coherent matrix. The final prepared slope would be a set of filled up boxes which are stacked on each other and act like a reinforced rock beam. It was found that, using geogrid boxes for stabilization of slopes causes cost reduction due to decrease in amount of excavation and labor cost, utilizing the in-situ materials, as well as reduction in construction time. It was also reported that GBM allows the slope to stand at steeper angle.

Recently, in a related study, the authors (Moradi extended the application of this technique for stabilization of rock-soil materials and investigated whether this new approach is more effective than the commonly practiced layered geogrid method (LGM). The results showed that the GBM reinforcement brings four additional advantages:

1- increasing the ultimate bearing capacity: based on the vertical spacing of geogrids; the ultimate bearing capacity of the GBM could be 11.16% higher than that of the LGM;

2- increasing the stiffness of the sand bed;

3- enhancing drainage efficiency;

4- saving in the land space to construct a reinforced sand bed system.

The present work aims to experimentally and numerically analyze the bearing capacity and settlement behavior of circular footing resting on GBM-reinforced rock-soil slopes and to evaluate the scale effects on the response of the reinforced rock-soil system.

2. Materials and characterization

2.1 Rock-soil materials

The rock-soil materials used in this work was obtained

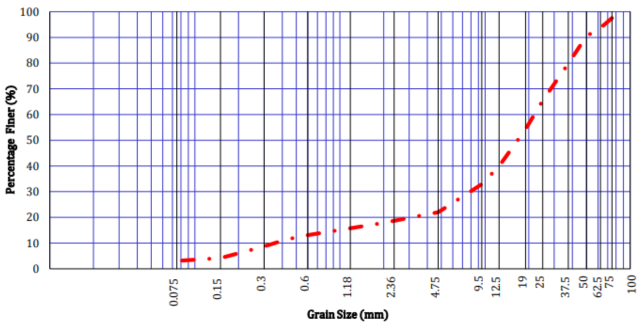

Fig. 1 Grain size distribution of rock-soil materials

Table 1 Rock-soil materials parameters

Parameter	Unit	Value	
		Loose	Dense
Unit weight of materials (γ)	kN/m^3	1.97	2.11
Modulus of elasticity (E)	kN/m^2	40000	60000
Internal friction angle (ϕ)	deg	40	45
Cohesion (c)	kN/m^2	5	7
Friction angle efficiency (E_φ)	%	100	98
Cohesion efficiency (E_c)	%	83	75
Poisson's ratio (ν)	--	0.27	0.27

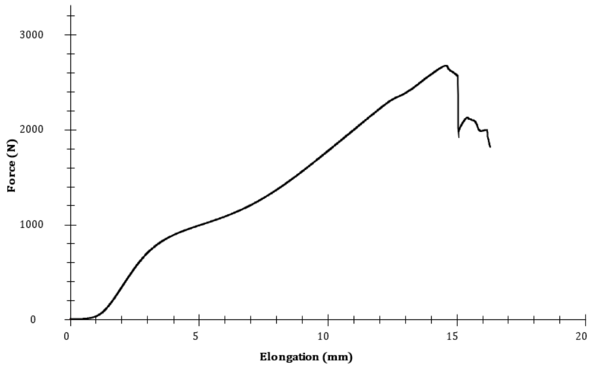

Fig. 2 Typical force-elongation curve of geogrid

Table 2 The engineering properties of geogrids

Reinforcement	Parameters	Unit	Value	Image
Geogrid A	Polymer	-	PVC Coated Polyester	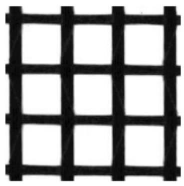
	Structure	-	Interwoven	
	Form	-	Sheet	
	Color	-	Black	
	Mass per unit area	g/m^2	220	
	Aperture dimensions	mm	25 × 25	
	UV resistance	%	> 93	
	Tensile strength	N	2675	
Geogrid B	Polymer	-	PVC Coated Polyester	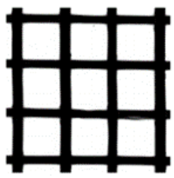
	Structure	-	Interwoven	
	Form	-	Sheet	
	Color	-	Black	
	Mass per unit area	g/m^2	186	
	Aperture dimensions	mm	25 × 25	
	UV resistance	%	> 93	
	Tensile strength	N	1774	
Geogrid C	Polymer	-	Polypropylene	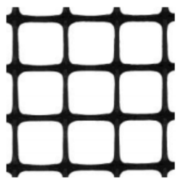
	Structure	-	Extruded	
	Form	-	Sheet	
	Color	-	Black	
	Mass per unit area	g/m^2	137	
	Aperture dimensions	mm	25 × 25	
	Tensile strength	N	1280	
Geogrid D	Polymer	-	Polypropylene	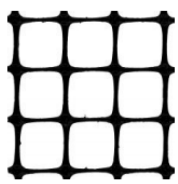
	Structure	-	Extruded	
	Form	-	Sheet	
	Color	-	Black	
	Mass per unit area	g/m^2	110	
	Aperture dimensions	mm	25 × 25	
	Tensile strength	N	813	

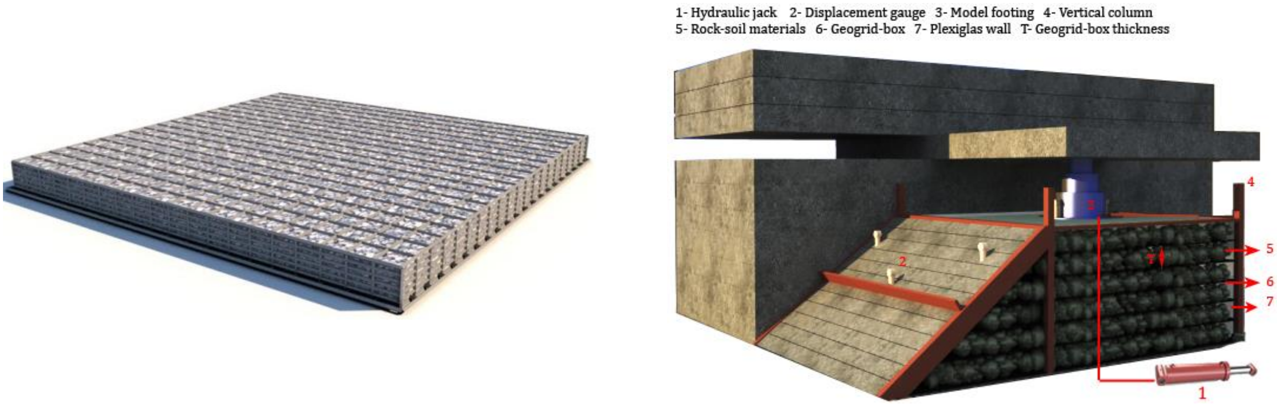

(a) (b)

Fig. 3 Schematic view of (a) geogrid-box and (b) slope model

from a slope in Hashtgerd-Iran. The sieve analysis tests were conducted according to ASTM D422-63. The grain size distribution curve of the materials is shown in Fig. 1.

The unit weight of investigated materials was determined using AASHTO - T180-D. The unit weight for loose- and dense-packing materials is presented in Table 1. In order to determine the shear strength of rock-soil materials, a series of direct shear tests were conducted. The values of internal friction angle (ϕ) and cohesion (c) are also presented in Table 1. The values of friction angle of rock-soil materials and geogrid (δ) and the adhesion of geogrid to rock-soil materials (c_a) were estimated according to ASTM-D5321. The friction angle efficiency (E_φ) and cohesion efficiency (E_c) were calculated using Eqs. (1)-(2). The results are presented in Table 1.

$$E_\varphi = \frac{\tan \delta}{\tan \varphi} \times 100 \tag{1}$$

$$E_C = \frac{c_a}{c} \times 100 \tag{2}$$

2.2 Geogrid

Two commercially available interwoven geogrids made of multifilament polyester (PET) yarns and two geogrids made of polypropylene (PP) with aperture size of 25 mm×25 mm were used as reinforcing material. The exterior surface of PET geogrids is coated with an additional thin protective layer of polyvinyl chloride (PVC) to increase ultraviolet, acid, and alkali resistance. The geogrids were conditioned at 65 ± 2% relative humidity and 24 ± 2 $°C$ for 24 h and subsequently tested for tensile properties. To this end, according to ASTM D6637-0 the geogrids were subjected to uniaxial loading on a Zwick CRE tensile tester (model 1446, Germany) with gage lengths of 50 mm, strain rate of 10 mm/min and initial force of 5 N. For each sample, five tests were conducted. The setup completely housed in an enclosure and the tests were performed at a relative humidity of 65 ± 2% and temperature of 21 ± 2°C. The typical force-elongation curve of a geogrid is presented in Fig. 2. The geogrids properties are given in Table 2.

3. Physical model and sample preparation

A series of laboratory model tests were performed in a steel frame test tank to investigate the effect of scale on bearing capacity behavior of rock-soil slopes. The physical models were constructed 760, 990, 1290 and 1670 mm in height and 1000 mm×1000 mm in width with a slope inclination angle (α) of 60°. The dimensions were chosen based on the literature studies and the results of the finite element analysis (FEA) conducted prior to the model tests. One sidewall of the model was built using a 10 mm thick transparent Plexiglas. The Plexiglas side allows the observation and photogrammetry of the failure modes and deformations of the geogrid-reinforced rock-soil during preparation and loading. The interior walls of the test tank were polished smooth using galvanized coat in the inside walls to minimize side friction with the rock-soil materials. Possible friction between the Plexiglas wall and the artificially made ground was minimized by attaching the transparency films onto the inside walls. For each test, new films were used to remove the possible effect of scratches. In order to maintain plane strain conditions and minimize out-of-plane displacements, the tank was built sufficiently rigid using four vertical columns and two horizontal profiles. A schematic illustration of geogrid-box, slope model and test configuration is presented in Fig. 3.

The proposed testing geometry of the slope was first marked on the transparent wall for reference. The thickness of geogrid-box was taken as 200 mm. To evaluate the effect of rock-soil stiffness on bearing capacity and the failure mechanism of rock-soil slope reinforced with geogrid-box, both loose- and dense-packing modes were investigated. The average unit weight (γ) equal to 19.7 kN/m^2 was decided for the loose mode, whereas it was defined as 21.1 kN/m^2 for the dense-packing mode. This was achieved in the test tank using a carefully controlled raining technique. For the loose mode, according to the ASTM D1556 rock-soil materials were pluviated using a constant deposition height in layers of 50 mm thick through a raining device that is moved to and fro to spread the materials uniformly. A series of trials were run to determine the most favorable conditions and height of raining before the target unit weight could be achieved. The test showed that a falling height of 200 mm had to be maintained to achieve a dry unit weight of 19.7 kN/m^2. In order to make assure of achieving the constant unit weight during raining, small containers with given volume were placed randomly at various locations in the test tank (El Sawwaf 2007). The pluviation process continued until the marked height (H) of the slope was reached. After preparing the slope up to a preassigned height in the test tank, the top surface was scraped and properly leveled by a sharp edge ruler to get as near as possible a flat surface so that the relative density of the top surface was not affected. To fill up the experimental design in the dense-packing mode, according to the ASTM D1556, the material was poured into the experimental design using raining technique in layers of 50 mm thick. Each layer was tamped using a standard hammer with a weight of 10 kg dropping from 200 mm height 25 times, then the surface of the layer was leveled and the next layer was located over the flattened layer. The procedure was then continued in a similar manner until the desired height was reached. It must be pointed out that, the lower layers located in the bottom of test tank are subjected to more compactness due to the tamping action of hammer on the upper layers. In this manner, if the same drop height for rock-soil materials in all steps of compaction is assessed, the sample would have higher unit weight in the lower layers. Consequently, in order to have an equal compaction approximately from top to bottom of sample, according to the work of Ladd (1978) and Tavangar and Shooshpasha (2016) the lower layers have higher fall height than the upper ones. After preparation, the rock-soil materials were carefully leveled in the areas directly beneath the footing. This was to ensure that the model footing had full contact with the rock-soil materials and the load was vertically applied to the foundation. To ensure standardized conditions throughout the investigation, at the end of each test, all rock-soil materials were removed completely from the test tank and the same procedure was repeated for a new test.

4. Experimental setup and testing program

A normal compressive static load (P) was applied on the slope through an integrated system of hydraulic jack, high-pressure water hose, force gauge, manual pump, load weight, and circular loading plate. The occurred displacements were measured using six magnetic based dial gauges with an accuracy of 0.01 mm. Prior to the experimental tests, numerical analysis was conducted to detect the critical points in terms of strain variations (Fig. 4) and the displacement gauges were installed at these points.

Displacement gauges 1, 2, and 3 were installed at 120° intervals located at equal distances from the center of the footing, and averaged to get the settlement of the footing. Displacement gauges 4, 5, and 6 were installed on the slope face. The displacement gauges were calibrated before each loading cycle. A schematic view of load application setup and the position of displacement gauges in the physical model are displayed in Fig. 3.

Loading tests were performed using a circular footing plate in 30 mm thickness to provide the rigid footing condition. The diameter of footing was selected as 300 mm. A thin layer of sand was cemented to the bottom surface of footing using epoxy glue to ensure uniform roughness in all the tests. The footing was placed on the surface of the sand bed at predetermined locations and the vertical compressive load was applied incrementally by means of a motor-controlled hydraulic jack at a rate of 0.5 mm/min with corresponding loading increment of 25 kPa. The loading rate was monitored using a calibrated load cell. The settlements in the critical parts of the slope were recorded using displacement gauges at the end of each increment. Each load increment was kept constant until the footing settlement was stabilized, around for 8-10 minutes. The loading increment continued until either a noticeable reduction in the applied vertical load is observed or a relatively slight increase in the vertical load results in a considerable settlement of footing. Each test was repeated up to five times to ensure the repeatability of the results and to achieve some degree of confidence with a limit of repeatability ±10% in the ultimate bearing capacity.

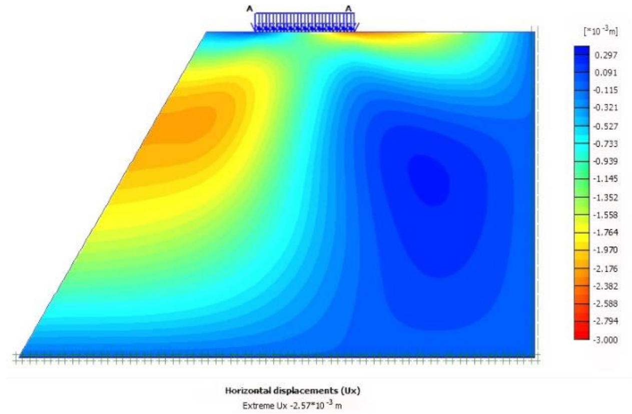

Fig. 4 The critical points in terms of strain variations

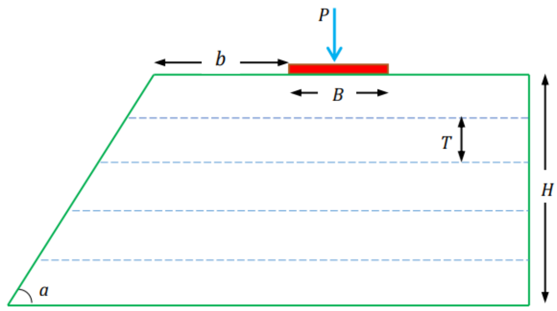

Fig. 5 Schematic illustration of variable parameters

In this study, 34 test programs and experimental tests were performed to investigate the inclusion effect of GBM on the bearing capacity and failure mechanism of rock-soil slopes. This GBM works based on the confining reinforcement theory. This confinement not only increases the friction angle of the materials, but also results in a drainage system to maintain slope stability (Fahimifar *et al.* 2014). In order to study the scale effects on the bearing capacity and failure mechanism, various test programs were considered and tests were conducted to investigate the effect of footing location, slope height (H) and geogrid tensile strength in loose- and dense-packing modes. Each

Table 3 Summary of experimental and numerical testing program

Test Series	Reinforcement	Constant Parameters	Variable Parameters	Value	Design
I	Unreinforced	$B/b = 0.5,\ \alpha = 60°$, Loose-packing, $T = 200\ mm$	H	760 mm	1
				990 mm	2
				1290 mm	3
				1670 mm	4
II	Unreinforced	$B/b = 0.5,\ \alpha = 60°$, Dense-packing, $T = 200\ mm$	H	760 mm	5
				990 mm	6
				1290 mm	7
				1670 mm	8
III	Unreinforced	$\alpha = 60°,\ H = 990\ mm$, Dense-packing, $T = 200\ mm$	B/b	0	9
				1	10
				1.5	11
				2	12
IV	Reinforced	$B/b = 0.5,\ \alpha = 60°$, Loose-packing, Geogrid A, $T = 200\ mm$	H	760 mm	13
				990 mm	14
				1290 mm	15
				1670 mm	16
V	Reinforced	$B/b = 0.5,\ \alpha = 60°$, Dense-packing, Geogrid A, $T = 200\ mm$	H	760 mm	17
				990 mm	18
				1290 mm	19
				1670 mm	20
VI	Reinforced	$\alpha = 60°,\ H = 990\ mm$, Dense-packing, Geogrid A, $T = 200\ mm$	B/b	0	21
				1	22
				1.5	23
				2	24
VII	Reinforced	$\alpha = 60°,\ H = 990\ mm$, Loose-packing, Geogrid A, $T = 200\ mm$	B/b	0	25
				1	26
				1.5	27
				2	28
VIII	Reinforced	$B/b = 0.5,\ \alpha = 60°$, $H = 990\ mm$, Dense-packing, $T = 200\ mm$	Geogrid type	B	29
				C	30
				D	31
IX	Reinforced	$B/b = 0.5,\ \alpha = 60°$, $H = 990\ mm$, Loose-packing, $T = 200\ mm$	Geogrid type	B	32
				C	33
				D	34

* B= footing diameter, b= horizontal distance between the footing and the slope crest, α= slope angle, H= slope height and T= Geogrid-box thickness

test was carried out to study the effect of one parameter while the other variables were kept constant. The physical model of rock-soil slope reinforced with geogrid-box was examined at four different heights and two densities namely loose- and dense- packing. Moreover, to evaluate the effect of proximity of footing to the slope crest (B/b), the loading was performed at five different distances form the edge of the slope. The parameter b is the horizontal distance between the footing and the slope crest and B is the footing diameter and is constant for all experiments. Additionally, in order to investigate the effect of geogrid tensile strength, four geogrids with different tensile strength and same aperture size were used. Eventually, the ultimate bearing capacity, failure mechanisms, settlement behavior and safety factor for all designs were evaluated and compared with those of unreinforced slopes. It must be pointed out that before carrying out the tests, the effect of box thickness (T) on bearing capacity and safety factor of the slopes was investigated. As far as these two parameters are concerned, the reinforced slopes exhibited the best performance for $T = 200\ mm$. Hence, the optimal thickness of box was considered $200\ mm$ in all designs.
Totally, 9 series of tests were organized and performed to study the effect of GBM on bearing capacity and settlement behavior of rock-soil slopes. Fig. 5 shows the schematic illustration of variable parameters and Table 3 summarizes the details of various test configurations considered in this study.

The primary purpose of series I and II is to evaluate the effect of slope height on bearing capacity behavior of unreinforced rock-soil slopes in loose- and dense-packing modes, respectively. Series III were performed to study the effect of footing location on bearing capacity behavior of unreinforced slopes. Series IV and V were planned to investigate the effect of slope height on bearing capacity behavior of GBM-reinforced rock-soil slopes in loose- and dense-packing modes, respectively. Series VI and VII were designed to investigate the effect of footing location on performance of GBM-reinforced slopes in dense- and loose-packing modes, respectively. Series VIII and IX were planned to investigate the effect of geogrid tensile strength on bearing capacity behavior of GBM-reinforced slopes in dense- and loose packing modes.

5. Numerical analysis

In order to validate the laboratory model tests results and provide insights into the internal deformations trends within the reinforced and unreinforced rock-soil materials, some three-dimensional finite element analysis (FEA) were performed on a footing-slope system. The analyses were performed using the finite element program, ABAQUS software. The advantage of developing such a FEA model is that it can be used to model a broad range of conditions which have not been examined experimentally. The geometry of the model footing-slope system and slope angle was assumed to be the same as the laboratory model. The material of steel plate for footing, geogrid and rock-soil, and loading plate dimensions were the same as those assigned in laboratory tests. Solid element and Mohr Coulomb (MC) model were used respectively to model rock-soil material and describe the elastic-plastic behavior of materials. The loading plate was modeled using the Solid element with elastic behavior and steel characteristics. A "Tie" constraint was set at the footing-soil interface to simulate rough contact between the footing and soil and no-slip was allowed at the interface between bottom surface of

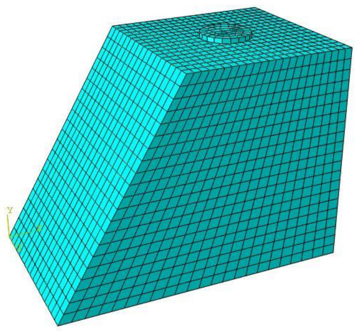

(a)

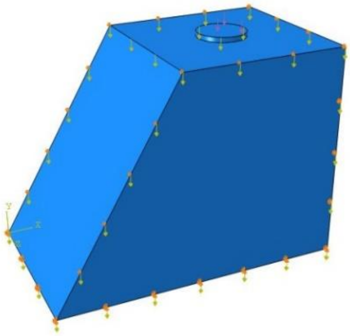

(b)

Fig. 6 (a) The geometry and generated mesh of the slope model and (b) boundary conditions

Table 4 Rock-soil materials parameters in numerical analysis

Parameter	Unit	Value	
		Loose	Dense
Unit weight of materials (γ)	kN/m^3	1.97	2.11
Stiffness modulus for primary loading (E_{50}^{ref})	kN/m^2	40000	60000
Stiffness modulus for unloading-reloading (E_{ur})	kN/m^2	1.2×10^5	1.8×10^5
Internal friction angle (ϕ)	deg	40	45
Cohesion (c)	kN/m^2	5	7
Poisson's ratio (ν)	--	0.27	0.27

footing and soil. The geogrid was modeled using the Shell element with plastic behavior with a pure tension. The interaction between the geogrid and surrounding rock-soil materials was modeled at both sides using the interface elements to describe more realistically the geogrid behavior. The interaction between the geogrid and soil was modeled using the embedded element technique. This technique is used to specify a group of elements that lie embedded in a group of host elements whose response will be used to constrain the translational degrees of freedom of the embedded nodes (i.e., nodes of embedded elements). The accuracy of the model was improved by using hexagonal and quad elements for Solid and Shell elements, respectively. A refined mesh was adopted to minimize the effect of mesh dependency on the FEA modeling. Prior to applying the load to the slope, the initial stress conditions were defined and the corresponding displacements were set to zero. The slope geometry, generated mesh, and boundary conditions are presented in Fig. 6. The input parameters for numerical analysis of rock-soil material are presented in Table 4.

6. Results and discussion

To evaluate the settlement behavior of rock-soil slope, the average settlement recorded by displacement gauges 1, 2, and 3 installed on the loading plates were measured in each loading stage (S). The footing settlement (S) was expressed in dimensionless form in terms of footing diameter (B) as the settlement ratio (S/B). In this section, the relation of vertical pressure loading with settlement ratio $(P-S/B$ plots) for various designs is presented and discussed.

A noticeable uplift deformation can also provide an indication of slope failure initiation. The average uplift in each loading stage (U) was measured using the displacement gauges 4, 5, and 6 installed on the slope face. It must be pointed out that at all loading stages, the measured displacements by gauge 6 (located in the center of the slope face) were much lower than those measured by gauges 4 and 5. This is attributed to the fact that, displacement gauges 4 and 5 are installed in the proximity of the slope solid walls and have greater distance from the center of the slope face as compared with displacement gauge 6.

In order to evaluate the reinforcement effects of GBM on the bearing capacity behavior of rock-soil slopes, the dimensionless parameters BCR and BCR' were defined using Eqs. (3)-(4).

$$BCR = \frac{P_{UR}}{P_U} \tag{3}$$

$$BCR' = \frac{P'_{UR}}{P'_U} \tag{4}$$

where BCR and BCR' denote the bearing capacity ratios obtained through laboratory model tests and numerical analysis, respectively. P_{UR} and P'_{UR} are the ultimate bearing capacity of the GBM-reinforced slopes in the laboratory and numerical models, respectively; and P_U and P'_U are the ultimate bearing capacity of unreinforced slopes in the laboratory and numerical models, respectively. The BCR is commonly used to express and compare the tests data of the reinforced and unreinforced soils at a known settlement.

When determining the ultimate bearing capacities using the $P-S/B$ curves from the finite element analyses, a footing pressure producing a footing settlement of 10% of the footing diameter (i.e., $0.1B$) at the footing center was taken as the ultimate bearing capacity (Yoo 2001, El Sawwaf 2007).

6.1 Effect of packing mode in unreinforced slopes

Series I and II investigate the behavior of unreinforced rock-soil slopes for the loose- and dense-packing modes,

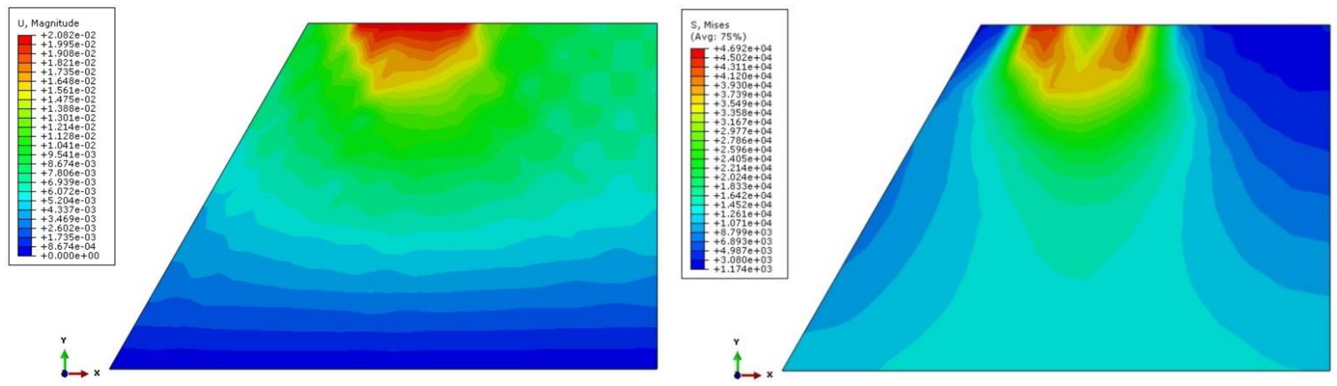

(a) (b)

Fig. 7 (a) Displacement contours and (b) stress contours for the unreinforced slope in loose-packing mode (design 2)

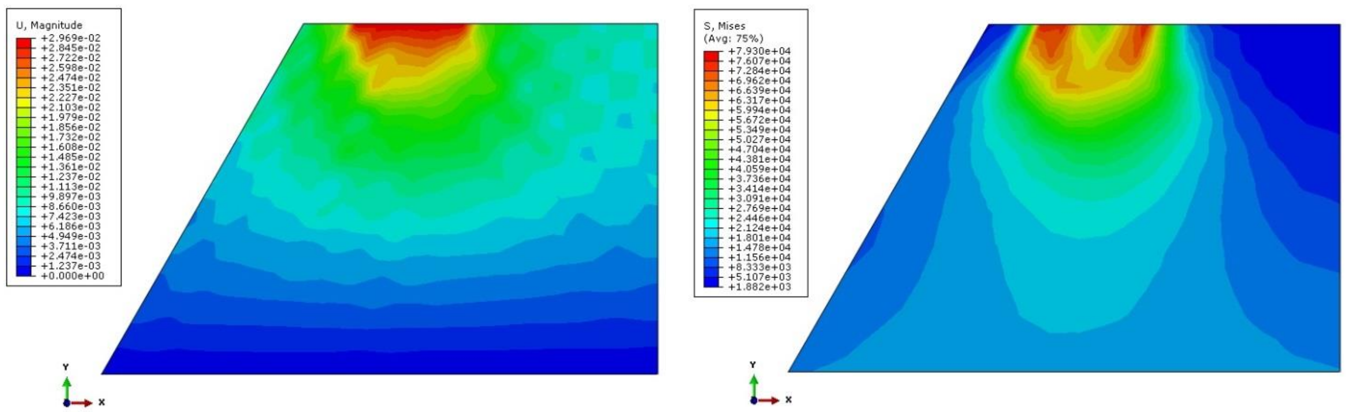

(a) (b)

Fig. 8 (a) Displacement contours and (b) stress contours for unreinforced slope in dense-packing mode (design 6)

respectively. Fig. 7 depicts the displacement and stress contours for the unreinforced slope with height of 990 mm in loose mode under loading of a circular footing (design 2). As can be observed, the displacement contours are very shallow and concentrated underneath the footing. Hence, a limited area of rock-soil materials resists the applied load, leading to the very low bearing capacity of the slope as observed in Fig. 7(b).

In Fig. 8, the displacement contour for the unreinforced dense rock-soil slope with height of 990 mm is shown (design 6). The figure shows that the displacement contours in dense-packing mode have distributed wider and deeper as compared with the loose mode. This is attributed to the higher stiffness and angle of friction of dense rock-soils as compared with the loose rock-soils. In fact, an increase in the unit weight is accompanied by the increased stiffness of the material. This results in the distribution of stresses in a broader and deeper area, which causes a larger mass of rock-soil materials resist the applied load and hence increasing the bearing capacity of the slope as observed in Fig. 8(b) and Fig. 9. The failure in both designs 2 and 6 is circular and failure wedge develops from the slope crest to the toe.

6.2 Effect of reinforcement

Fig. 9 shows variations of pressure load with bearing capacity ratio for designs 2, 6, 14 and 18. As is observed, a good agreement between the results of laboratory model with those of numerical models exists. When dense-packing rock-soil materials are subjected to vertical pressure loading, a maximum value of $P = P_u$ is clearly defined in the load-settlement curve. In other words, as can be observed in Fig. 9 the ultimate bearing capacity (P_u) would be distinctly evident in the peak of the load-settlement curve and the general shear failure is the governing mode of failure. This behavior was not observed in any of the GBM-reinforced laboratory tests and numerical analysis for loose mode. This may be ascribed to the loose-packing nature of rock-soil materials and presence of voids within the aggregates (Alamshahi and Hataf 2009, Fattah *et al*. 2014). Therefore, the increase in loading results in the settlement of aggregates and hence, no peak is observed in the load-settlement curve. In these cases, choosing a single value of ultimate bearing capacity may be highly subjective. Hence, in order to make the results comparable, the ultimate bearing capacity was taken as the point at which the settlement reaches 10% of the footing diameter; i.e., $0.1\ B$.

Fig. 9 shows that inclusion of geogrid-box considerably increases the ultimate bearing capacity of rock-soil slopes for the loose- and dense-packing modes. These observations are attributed to the reinforcement mechanism which is derived from the passive earth resistance and interlocking

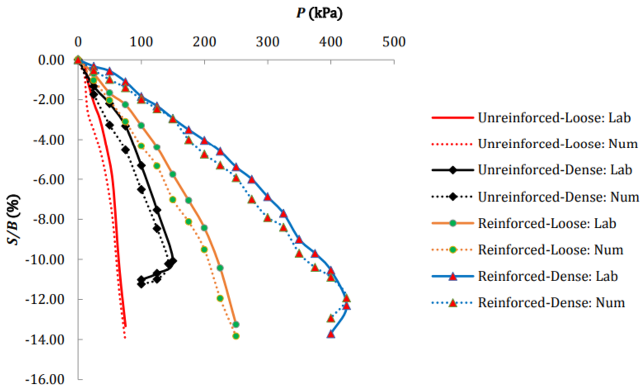

Fig. 9 Variations of pressure load with bearing capacity ratio for designs 2, 6 14 and 18

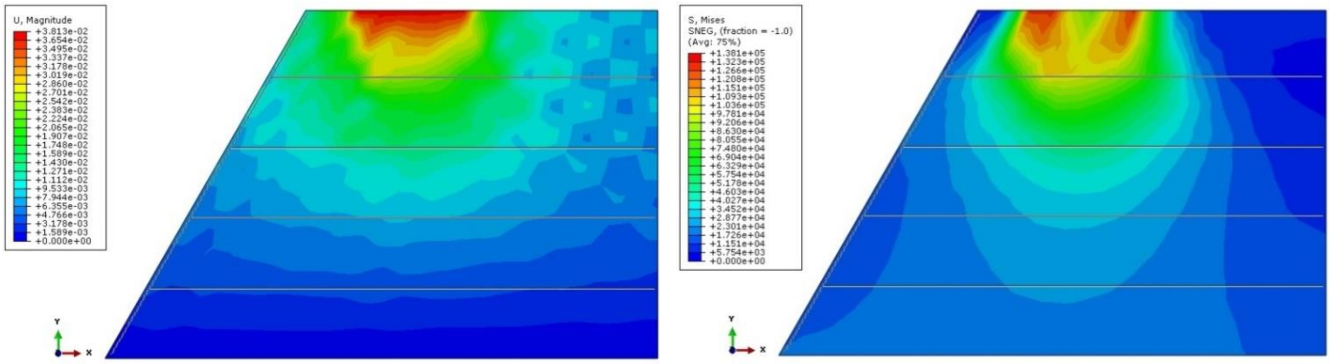

(a) (b)

Fig. 10 (a) Displacement contours and (b) stress contours for reinforced slope in loose-packing mode (design 14)

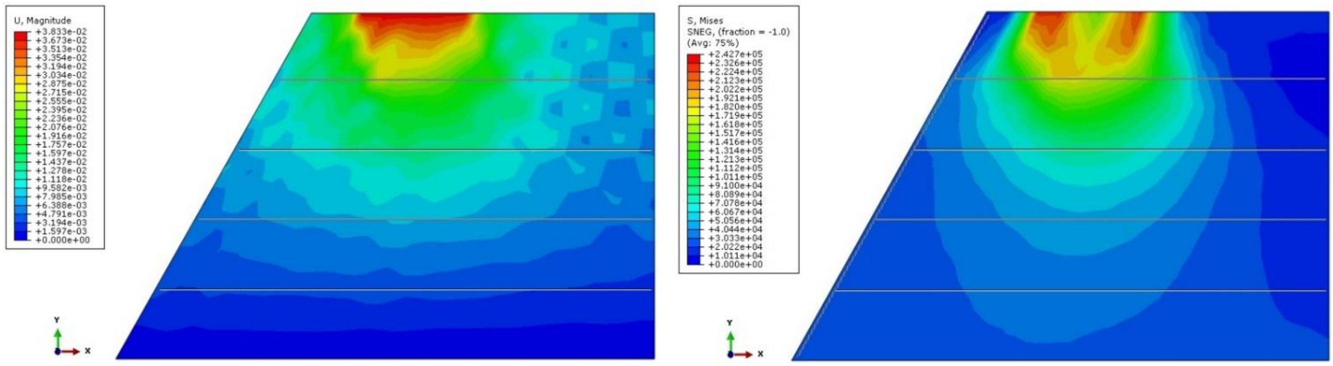

(a) (b)

Fig. 11 (a) Displacement contours and (b) stress contours for reinforced slope in dense-packing mode (design 18)

action between the rock-soil materials and the reinforcement (El Sawwaf 2007, Tavakoli *et al*. 2016). The mechanical interlock creates the confinement effect of reinforcement and enables the geogrid to resist horizontal shear stresses from the loaded plate. This results in even distribution of vertical pressure in a wider and deeper area as seen in Figs. 10-11, which in turn increases the bearing capacity of the slope. Additionally, the geogrid-boxes restrict lateral movement of rock-soil materials toward the slope face and push them downward in greater depth. This in turn results in spreading the footing load in a wider and deeper area into the soil which means a longer failure surface and greater bearing capacity (El Sawwaf 2010). For both the reinforced loose and dense rock-soil slopes, at the ultimate bearing load the slopes experience some cracking; however, the deformations were not so extensive that undermined the integrity of the structure.

Comparison of designs 14 and 18 shows that the reinforced slopes in the dense-packing mode enjoy higher bearing capacity as compared with the loose mode. This is attributed to the higher relative density of rock-soil materials in the dense-packing mode. As the relative density increases, the angle of friction of the rock-soil materials increases, and hence the adhesion, friction, and interlocking between soil and reinforcement increases leading to a greater bearing capacity (Prasad *et al*. 2016).

Based on the outputs of laboratory tests, the bearing capacity ratios for designs 14 and 18 are 3.21 and 2.83, respectively. These results indicate that the GBM is more efficient for reinforcement of rock-soil slopes in the loose-packing mode.

6.3 Effect of slope height in the loose-packing mode

To evaluate the effect of slope height on bearing capacity of slopes in the loose mode, the laboratory and numerical analysis were conducted at four slope heights including 760, 990, 1290 and 1670 mm (designs 13-16). In all designs, the B/b ratio is 0.5 and the thickness of geogrid box is 200 mm. Fig. 12 depicts typical variation of pressure load with settlement ratios for reinforced slopes for the laboratory and numerical modelings. Displacement contours were not presented for the sake of brevity.

As previously stated, for the dense-packing materials subjected to vertical pressure, P_u would be distinctly observed in the peak of the load-settlement curve and the shape of load-settlement curves indicates that general shear failure is the governing mode of failure. This behavior was not observed in any of the GBM-reinforced slopes in the loose-packing mode. Therefore, the increase in loading results in the footing settlement and thereby no peak is observed in the load-settlement curve. The shape of load-settlement curves indicates that punching and local shear failure is the governing mode of failure. Hence, in order to make the results comparable, P_u was taken as the point at which the settlement reaches 10% of the footing diameter. As can be observed, by increasing the slope height both the initial stiffness (initial slope of the $P-S/B$ curves) and the bearing load at the same settlement level decreases. This is consistent with the truth in reality that the higher of the slope, the more possible of failure. The measured ultimate bearing load of circular footing resting on GBM-reinforced slope with height of 760 mm in loose-packing mode is 347.6 kPa. This means that when the stress is 347.6 kPa, the average settlement recorded by gauges 1, 2, and 3 exceeds 10% of the loading plate diameter. For a settlement ratio equal to 10 %, the bearing loads for the slopes with heights of 990, 1290 and 1670 mm are 221.9, 144.26 and 122.3 kPa, respectively.

Fig. 12 also shows a good agreement between the laboratory and numerical results in all cases. Fig. 13 reveals the effect of slope height on bearing capacity ratio in the laboratory and numerical modeling. The value of BCR ranges from 2.91 to 5.81 and BCR increases with increasing the slope height. As illustrated, although the BCR values for numerical models appear to be higher than those for the laboratory models, the general trends of the manner in which BCR varies with the slope height are in good agreement.

6.4 Effect of slope height in the dense-packing mode

In order to analyze the effect of slope height on bearing capacity and settlement behavior of rock-soil slopes in the dense-packing mode, test series V (designs 17-20) were planned. The results of physical models together with numerical models are presented in Fig. 14. It must be pointed out that the numerical results for designs 19 and 20

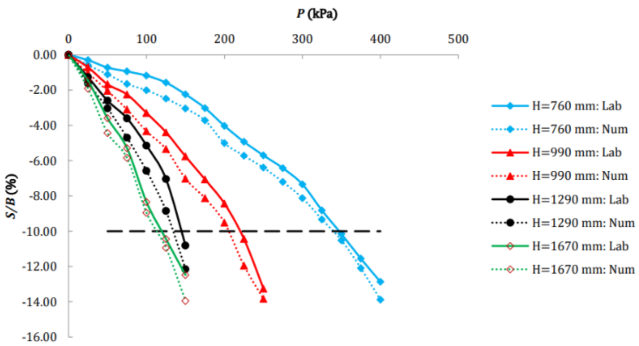

Fig. 12 Variations of pressure load with settlement ratio for reinforced slopes with different heights in loose-packing mode

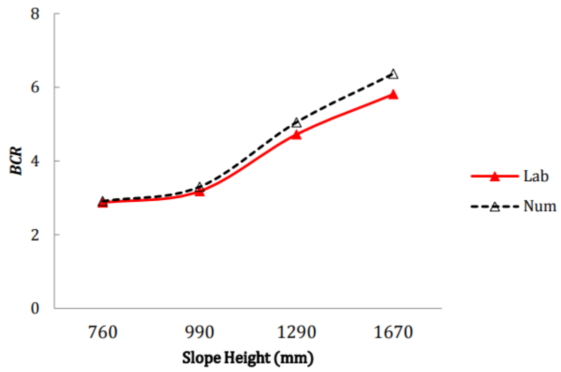

Fig. 13 Variation of BCR with the slope height in loose-packing mode

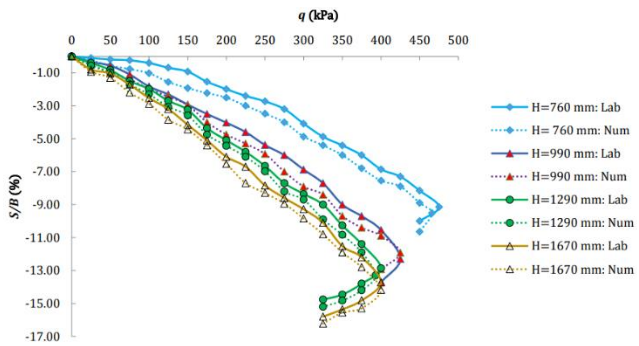

Fig. 14 Variations of pressure load with settlement ratio for slopes with different heights in dense-packing mode

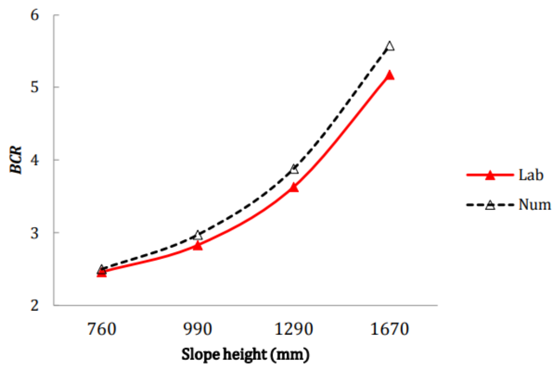

Fig. 15 Variation of BCR with the slope height in dense-packing mode

were not plotted for clarity; however, in all cases a good agreement between the laboratory and numerical results was observed.

As can be seen, for all cases the ultimate bearing capacity (P_u) is clearly defined in the peak of the load-settlement curve. The results indicate that the GBM significantly improves the bearing capacity and settlement behavior of rock-soil slopes. The results also indicate that by increasing the slope height from 760 mm to 1670 mm, the ultimate bearing load converges to 393 kPa. Fig. 14 illustrates that decreasing the slope height results in improving both the initial stiffness and bearing load at the same settlement level. However, the improvement in bearing capacity is accompanied by a decrease in settlement ratio. Comparison of Figs. 12-14 shows that at the same slope height, dense rock soil slopes enjoy higher ultimate bearing load as compared with the loose mode.

Fig. 15 illustrates the effect of slope height in the dense-packing mode on bearing capacity ratio in the laboratory and numerical modeling. As seen, there is a sharp increase in BCR with increasing the slope height. A good consistency is observed between the laboratory and numerical results. Comparison of Figs. 13-15 shows that at the same slope height, rock-soil slopes in loose-packing mode enjoy higher BCR values as compared with the dense-packing mode. This points to the fact that the maximum benefit of GBM reinforcement is obtained for rock-soil slopes in loose-packing mode.

6.5 Effect of footing location in dense- and loose-packing modes

Distance of the footing to the slope crest is one of the most profound factors in bearing capacity behavior of slopes. In order to evaluate the effect of footing location (B/b) on bearing capacity behavior three series of tests were performed on circular footing resting on rock-soil slopes. While the first was performed on unreinforced slopes, the second and third were carried out on GBM-reinforced slopes with height of 990 mm in the dense- and loose-packing modes, respectively. The distance of footing to the slope crest (B/b), was varied as 0, 0.5, 1, 1.5 and 2. For both the dense- and loose-packing modes, the results indicate a significant increase in the ultimate bearing load as the distance of the footing to the slope crest increases. This is ascribed to the soil passive resistance from the slope side and reinforcement effect. The more the distance of the footing to the slope crest is, the greater the passive resistance from the slope side to the failure wedge underneath the footing is. Additionally, as discussed in previous sections, inclusion of geogrid-box limits the lateral displacements of soil underneath the footing and confines the soil leading to a wider and deeper failure zone, which in turn results in significant decrease in vertical settlement and hence improves the ultimate bearing load (El Sawwaf 2010).

Fig. 16 shows variation of BCR with footing location with respect to the slope crest for the dense- and loose-packing modes. As can be observed, BCR significantly increases as the footing location moves closer to the slope crest. In other words, the maximum benefit of GBM reinforcement is obtained when the footing is placed at the slope crest. It can also be observed that, the GBM is more effective for the reinforcement of loose rock-soils, especially at lower distances. As the footing location moves away from the slope crest, for both the loose- and dense-packing modes the rate of decrease in BCR become less until a value of about $B/b = 1.5$, after which the BCR can be considered almost constant. As is observed, although the BCR values for numerical models appear to be higher than those for the laboratory models, the general trends of the manner in which BCR varies with foting location are in good agreement.

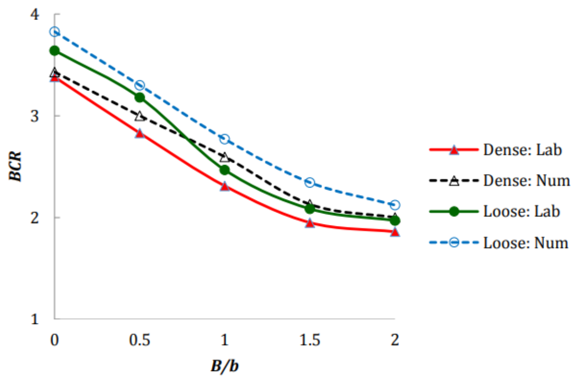

Fig. 16 Variation of BCR with footing location

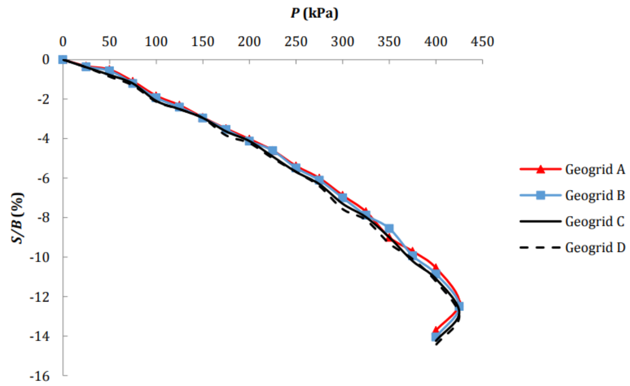

Fig. 17 Variations of pressure load with settlement ratio for slopes reinforced with different geogrids in dense-packing mode

6.6 Effect of geogrid tensile strength in dense- and loose-packing modes

In order to evaluate the effect of geogrid tensile strength on the bearing capacity behavior of dense- and loose rock-soil slopes reinforced with GBM, test series VIII and IX were performed, respectively. The tensile strength values of geogrids considered in this study are 2675, 1774, 1280 and 813 kN, which are typical for available geogrid products in the market. All the geogrids have aperture dimensions of 25 mm × 25 mm. Fig. 17 depicts typical variation of pressure load with settlement ratios for reinforced slopes with geogrids of different tensile strength in dense-packing mode. As can be observed, there exists no difference between the load-settlement behavior of reinforced rock-soil slopes. This is due to the fact that the stress levels at small-scale are not so large that the maximum tensile strength of geogrids is reached. Therefore, for none of the geogrids failure occurs during the loading process. In other words, for the GBM-reinforced slopes, failure occurs as a result of soil-geogrid mass movement, rather than geogrid rupture. Similar results were obtained for the loose-packing mode and hence the load-settlement curves were not presented for the sake of brevity.

6.7 Effect of GBM reinforcement on safety factor

In this section, the effect of the GBM on safety factor of rock-soil slopes is assessed using the limit equilibrium (LE) and finite element (FE) analysis. LE and FE analysis were performed using commercially available software SLIDE and ABAQUS, respectively to predict the bearing capacity behavior of slopes. In Tables 5 and 6, the improvement percentage in safety factors are given for the slopes in the loose-and dense-packing modes, respectively.

The results indicate that, the calculated safety factors obtained using ABAQUS and SLIDE are different. This is ascribed to the analysis mode performed by these two software. ABAQUS is a FE-based software in which no pre-defined slip surface or inter-slice forces is required, while SLIDE is based on LE principles and the geometry and location of slip surface must a priori be defined. Additionally, in FE-based methods the possible slip occurs in a zone, while in SLIDE the slide surface is considered to be a narrow curve. Considering above, the FE-based methods seem to be more valid than the LE-based methods (Huang and Jia 2003, Alkasawneh *et al*. 2008, Gurocak Alemdag *et al*. 2008, Mahboubi *et al*. 2008, Viswanadham and Konig 2009).

The tables also compare the results obtained from various LE-based methods, namely Bishop's Simplified Method (BSM) (Bishop 1955), Janbu's Generalized Method (JGM) (Janbu 1954) and Spencer Method (SM) (Spencer 1967).

Tables 5 and 6 show the improvement percentage in safety factors in the loose- and dense-packing modes, respectively. As is observed, inclusion of geogrid-box results in a significant increase in the safety factor of rock-soil slopes. Comparison of the results indicates that the maximum improvements are occurred for the loose-packing soils.

6.8 Large-scale modeling

In previous sections the capability of ABAQUS software in investigation of failure behavior and load-settlement behavior of rock-soil slopes reinforced with GBM was assessed. The results point to the good agreement between the results of laboratory modeling with those of numerical modeling. This indicates the accuracy of ABAQUS software in assessment of the behavior of rock-soil slopes. In this section, a slope located in Hashtgerd-Iran was modeled using ABAQUS software and the effect of GBM on safety factor of the slope was investigated. Note that the rock-soil materials used in small-scale laboratory models were extracted from this slope and the used rock-soil materials and geogrids were the same for both the small- and large-scale analysis. Engineering geological properties of the rock-soil materials exposed in the case study slope were determined on the basis of field observations/measurements and laboratory tests. The slope height and width was 20 and 11 m respectively and the slope has the same inclination angle of model test slopes. The thickness of geogrid-box was considered 80 cm. The slope was modeled for the dense-packing mode. The improvement percentage in safety factors for the large-scale models is presented in Table 7. As is observed, GBM results a 31.5% increase in safety factor of rock-soil slopes. It must be pointed out that the GBM results in cost reduction due to the decrease in amount of excavation, omitting some of the machinery and utilizing the existence material in the place, as well as reduction in construction time (Fahimifar *et al*. 2014).

Table 5 Improvement percentage in safety factor for the slopes in loose-packing mode (design 2)

	ABAQUS	SLIDE		
		BSM	SM	JGM
Improvement (%)	88.59	88.13	90.59	91.78

Table 6 Improvement percentage in safety factor for the slopes in dense-packing mode (design 6)

	ABAQUS	SLIDE		
		BSM	SM	JGM
Improvement (%)	77.71	69.49	66.10	71.42

Table 7 Improvement percentage in safety factor for the real slopes in dense-packing mode

	ABAQUS	SLIDE		
		BSM	SM	JGM
Improvement (%)	31.54	29.12	27.86	29.31

7. Conclusions

A series of small-scale laboratory studies were conducted to obtain the load-settlement response of a model circular footing resting on unreinforced and reinforced rock-soil slopes. Several parameters including rock-soil materials density (loose- and dense-packing modes), slope height, location of footing relative to the slope crest and tensile strength of geogrids were studied. In order to supplement the results of the model tests and perceive internal deformation of reinforced and unreinforced rock-soil materials, a series of 3D FEA were performed using ABAQUS software. Additionally, in order to calculate the safety factor, LE and FE analysis were conducted using commercially available software SLIDE and ABAQUS, respectively. The following general conclusions are drawn from the study:

• The GBM significantly improves both the bearing capacity and settlement behavior of rock-soil slopes. This is ascribed to the reinforcement mechanism which was derived from the passive earth resistance and adhesion between the longitudinal/transverse geogrid members and the rock-soil materials, which in turn limits the spreading and lateral deformations of soil.

• The displacement contours in the dense-packing mode distributed in a wider and deeper area as compared with the loose-packing mode, leading to higher ultimate bearing load.

• In the loose-packing mode an increase in the vertical pressure load is accompanied with an increase in the soil settlement, while in the dense mode the ultimate bearing capacity (P_u) would be distinctly evident in the peak of the load-settlement curve and the load-settlement curves show a pronounced peak.

• Comparison of bearing capacity ratios for the dense- and loose-packing modes demonstrated that the maximum benefit of GBM is obtained for rock-soil slopes in loose-packing mode.

• Packing mode has paramount influence on the behavior of reinforced slope and leads to the change in modal behavior at failure state.

• By increasing the slope height, both the initial stiffness and the bearing load decreases. Additionally, BCR increases with increasing the slope height for both the loose and dense rock soils.

• A significant increase in the ultimate bearing load is observed as the distance of the footing to the slope crest increases. Additionally, BCR significantly increases as the footing location moves closer to the slope crest.

• GBM results in a significant increase in the safety factor of rock-soil slopes.

• Maximum improvements in safety factor are occurred for the loose-packing soils.

• High consistency was observed between the laboratory and numerical results.

Funding

This research did not receive any specific grant from funding agencies in the public, commercial, or not-for-profit sectors.

References

Abhishek, S., Rajyalakshmi, K. and Madhav, M. (2015), "Bearing capacity of strip footing on reinforced foundation bed over soft ground with granular trench", *Ind. Geotech. J.*, **45**(3), 304-317. https://doi.org/10.1007/s40098-014-0138-y.

Alamshahi, S. and Hataf, N. (2009), "Bearing capacity of strip footings on sand slopes reinforced with geogrid and grid-anchor", *Geotext. Geomembr.*, **27**(3), 217-226. https://doi.org/10.1016/j.geotexmem.2008.11.011.

Alejano, L., Pons, B., Bastante, F., Alonso, E. and Stockhausen, H. (2007), "Slope geometry design as a means for controlling rockfalls in quarries", *Int. J. Rock Mech. Min. Sci.*, **44**(6), 903-921. https://doi.org/10.1016/j.ijrmms.2007.02.001.

Alkasawneh, W., Malkawi, A.I.H., Nusairat, J.H. and Albataineh, N. (2008), "A comparative study of various commercially available programs in slope stability analysis", *Comput. Geotech.*, **35**(3), 428-435. https://doi.org/10.1016/j.compgeo.2007.06.009.

Ashtiani, M., Ghalandarzadeh, A. and Towhata, I. (2015), "Centrifuge modeling of shallow embedded foundations subjected to reverse fault rupture", *Can. Geotech. J.*, **53**(3), 505-519. https://doi.org/10.1139/cgj-2014-0444.

Ausilio, E., Conte, E. and Dente, G. (2001), "Stability analysis of slopes reinforced with piles", *Comput. Geotech.*, **28**(8), 591-611. https://doi.org/10.1016/S0266-352X(01)00013-1.

Berry, D.S. (1935), *Stability of Granular Mixtur*es, University of Michigan, Michigan, U.S.A.

Bishop, A.W. (1955), "The use of the slip circle in the stability analysis of slopes", *Geotechnique*, **5**(1), 7-17.

Bouassida, M., Jellali, B. and Lyamin, A. (2014), "Ultimate bearing capacity of a strip footing on ground reinforced by a trench", *Int. J. Geomech.*, **15**(3), 06014021. https://doi.org/10.1061/(ASCE)GM.1943-5622.0000418.

Cerato, A.B. and Lutenegger, A.J. (2007), "Scale effects of shallow foundation bearing capacity on granular material", *J. Geotech. Geoenviron. Eng.*, **133**(10), 1192-1202. https://doi.org/10.1061/(ASCE)1090-0241(2007)133:10(1192).

Chung, W. and Cascante, G. (2007), "Experimental and numerical study of soil-reinforcement effects on the low-strain stiffness and bearing capacity of shallow foundations", *Geotech. Geol. Eng.*, **25**(3), 265-281. https://doi.org/10.1007/s10706-006-9109-0.

Conte, E. and Troncone, A. (2018), "A performance-based method for the design of drainage trenches used to stabilize slopes", *Eng. Geol.*, **239**, 158-166. https://doi.org/10.1016/j.enggeo.2018.03.017.

Demir, A., Yildiz, A., Laman, M. and Ornek, M. (2014), "Experimental and numerical analyses of circular footing on geogrid-reinforced granular fill underlain by soft clay", *Acta Geotechnica*, **9**(4), 711-723. https://doi.org/10.1007/s11440-013-0207-x.

El Sawwaf, M. (2010), "Experimental and numerical study of strip footing supported on stabilized sand slope", *Geotech. Geol. Eng.*, **28**(4), 311-323. https://doi.org/10.1007/s10706-009-9293-9.

El Sawwaf, M.A. (2007), "Behavior of strip footing on geogrid-reinforced sand over a soft clay slope", *Geotext. Geomembranes*, **25**(1), 50-60. https://doi.org/10.1016/j.geotexmem.2006.06.001.

Fahimifar, A., Abdolmaleki, A. and Soltani, P. (2014), "Stabilization of rock slopes using geogrid boxes", *Arab. J. Geosci.*, **7**(2), 609-621. https://doi.org/10.1007/s12517-012-0755-7.

Fahimifar, A. and Soroush, H. (2005), "A theoretical approach for analysis of the interaction between grouted rockbolts and rock masses", *Tunn. Undergr. Sp. Technol.*, **20**(4), 333-343. https://doi.org/10.1016/j.tust.2004.12.005.

Fattah, M., Shlash, K. and Mohammed, H. (2014), "Bearing capacity of rectangular footing on sandy soil bounded by a wall", *Arab. J. Sci. Eng.*, **39**(11). https://doi.org/10.1007/s13369-014-1353-7.

Feng, S.J., Chen, Z.W., Chen, H.X., Zheng, Q.T. and Liu, R. (2018), "Slope stability of landfills considering leachate recirculation using vertical wells", *Eng. Geol.*, **241**, 76-85. https://doi.org/10.1016/j.enggeo.2018.05.013.

Gurocak, Z., Alemdag, S. and Zaman, M.M. (2008), "Rock slope stability and excavatability assessment of rocks at the Kapikaya Dam Site, Turkey", *Eng. Geol.*, **96**(1-2), 17-27. https://doi.org/10.1016/j.enggeo.2007.08.005.

Hataf, N. and Sadr, A. (2015), "Experimental, numerical and analytical study on conventional and innovative Grid-Anchor system in the pull-out test", *Geomech. Geoeng.*, **10**(3), 182-193. https://doi.org/10.1080/17486025.2014.933893.

Hou, J., Zhang, M.X., Dai, Z.H., Li, J.Z. and Zeng, F.F. (2017), "Bearing capacity of strip foundations in horizontal-vertical reinforced soils", *Geotext. Geomembranes*, **45**(1), 29-34. https://doi.org/10.1016/j.geotexmem.2016.07.001.

Huang, M. and Jia, C.Q. (2003), "Strength reduction FEM in stability analysis of soil Slopes subjected to transient unsaturated seepage", *Comput. Geotech.*, **36**(1-2), 93-101. https://doi.org/10.1016/j.compgeo.2008.03.006.

Janbu, N. (1954), *Application of Composite Slip Surface for Stability Analysis*, Stockholm, Sweden.

Keskin, M.S. and Laman, M. (2014), "Experimental and numerical studies of strip footings on geogrid-reinforced sand slope", *Arab. J. Sci. Eng.*, **39**(3), 1607-1619. https://doi.org/10.1007/s13369-013-0795-7.

Kumar, J. and Khatri, V. (2008), "Effect of footing width on bearing capacity factor N_γ for smooth strip footings", *J. Geotech. Geoenviron. Eng.*, **134**(9), 1299-1310. https://doi.org/10.1061/(ASCE)1090-0241(2008)134:9(1299).

Kusakabe, O., Yamaguchi, H. and Morikage, A. (1991), "Experiment and analysis on the scale effect of Nγ for circular and rectangular footings", *Proceedings of the International Conference on Centrifuge*, Boulder, Colorado, U.S.A.

Ladd, R. (1978), "Preparing test specimens using undercompaction", *Geotech. Test. J.*, **1**(1), 16-23. https://doi.org/10.1520/GTJ10364J.

Mahboubi, A., Aminpour, M. and Noorzad, A. (2008), "Conventional and advanced numerical methods of rock slope stability analysis, A comparison study, Gotvand Dam Right Abutment (Iran) case study", *Proceedings of the 12th International Conference of International Association for Computer Methods and Advances in Geomechanics (IACMAG)*, Goa, India, October.

Meyerhof, G.G. (1963), "Some recent research on the bearing capacity of foundations", *Can. Geotech. J.*, **1**(1), 16-26. https://doi.org/10.1139/t63-003.

Moradi, G., Abdolmaleki, A., Soltani, P. and Ahmadvand, M. (2018), "A laboratory and numerical study on the effect of geogrid-box method on bearing capacity of rock-soil slopes", *Geomech. Eng.*, **14**(9), 345-354. https://doi.org/10.12989/gae.2018.14.4.345.

Mosallanezhad, M., Hataf, N. and Ghahramani, A. (2008), "Experimental study of bearing capacity of granular soils, reinforced with innovative grid-anchor system", *Geotech. Geol. Eng.*, **26**(3), 299-312.

Naeini, S., Rabe, B.K. and Mahmoodi, E. (2012), "Bearing capacity and settlement of strip footing on geosynthetic reinforced clayey slopes", *J. Central South Univ.*, **19**(4), 1116-1124. https://doi.org/10.1007/s11771-012-1117-z.

Nareeman, B.J. (2012), "A study on the scale effect on bearing capacity and settlement of shallow foundations", *Int. J. Eng. Technol.*, **2**(3), 480-488.

Prasad, B.D., Hariprasad, C. and Umashankar, B. (2016), "Load-settlement response of square footing on geogrid reinforced layered granular beds", *Int. J. Geosynth. Ground Eng.*, **2**(4), 36. https://doi.org/10.1007/s40891-016-0070-6.

Puzrin, A.M., Gray, T.E. and Hill, A.J. (2015), "Significance of the actual nonlinear slope geometry for catastrophic failure in submarine landslides", *Proc. R. Soc. A Math. Phys. Eng. Sci.*, **471**(2175), 20140772. https://doi.org/10.1098/rspa.2014.0772.

Ranjbarnia, M., Fahimifar, A. and Oreste, P. (2015), "Practical method for the design of pretensioned fully grouted rockbolts in tunnels", *Int. J. Geomech.*, **16**(1), 04015012. https://doi.org/10.1061/(ASCE)GM.1943-5622.0000464.

Saleh Ahmadi, M. and Moghadam, P.N. (2017), "Effect of geogrid aperture size and soil particle size on geogrid-soil interaction under pull-out loading", *J. Text. Polymers*, **5**(1), 25-30.

Spencer, E. (1967), "A method of analysis of the stability of embankments assuming parallel interslice forces", *Geotechnique*, **17**, 11-26.

Srbulov, M. (2001), "Analyses of stability of geogrid reinforced steep slopes and retaining walls", *Comput. Geotech.*, **28**(4), 255-268. https://doi.org/10.1016/S0266-352X(00)00032-X.

Tavakoli, M.G., Ghanbari, A. and Mehdizadeh, H. (2016), "Experimental study on the behaviour of geogrid-reinforced slopes with respect to aggregate size", *Geotext. Geomembranes*, **44**(6), 862-871. https://doi.org/10.1016/j.geotexmem.2016.06.006

Tavangar, Y. and Shooshpasha, I. (2016), "Experimental and numerical study of bearing capacity and effect of specimen size on uniform sand with medium density, reinforced with nonwoven geotextile", *Arab. J. Sci. Eng.*, **41**(10), 4127-4137. https://doi.org/10.1007/s13369-016-2101-y.

Touze-Foltz, N., Bannour, H., Barral, C. and Stoltz, G. (2016), "A review of the performance of geosynthetics for environmental protection", *Geotext. Geomembranes*, **44**(5), 656-672. https://doi.org/10.1016/j.geotexmem.2016.05.008.

Turker, E., Sadoglu, E., Cure, E. and Uzuner, B.A. (2014), "Bearing capacity of eccentrically loaded strip footings close to geotextile-reinforced sand slope", *Can. Geotech. J.*, **51**(8), 884-895. https://doi.org/10.1139/cgj-2014-0055.

Ukritchon, B., Whittle, A.J. and Klangvijit, C. (2003), "Calculations of bearing capacity factor N_γ using numerical limit analyses", *J. Geotech. Geoenviron. Eng.*, **129**(5), 468-474. https://doi.org/10.1061/(ASCE)1090-0241(2003)129:6(468).

Unnikrishnan, N. and Rajan, S. (2012), "Bearing capacity of strip footings on geosynthetic encapsulated granular trenches", *Proceedings of the International Conference on Ground Improvement and Ground Control*, Wollongong, Australia, October-November.

Viswanadham, B.V.S. and Konig, D. (2009), "Centrifuge modeling of geotextile-reinforced slopes subjected to differential settlements", *Geotext. Geomembranes*, **27**(2), 77-88. https://doi.org/10.1016/j.geotexmem.2008.09.008.

Won, J., You, K., Jeong, S. and Kim, S. (2005), "Coupled effects in stability analysis of pile-slope systems", *Comput. Geotech.*, **32**(4), 304-315. https://doi.org/10.1016/j.compgeo.2005.02.006.

Xiao, S., Feng, W. and Zhang, J. (2010), "Analysis of the effects of slope geometry on the dynamic response of a near-field mountain from the Wenchuan Earthquake", *J. Mountain Sci.*, **7**(4), 353-360. https://doi.org/10.1007/s11629-010-2055-6.

Xu, D.S. and Yin, J.H. (2016), "Analysis of excavation induced stress distributions of GFRP anchors in a soil slope using distributed fiber optic sensors", *Eng. Geol.*, **213**, 55-63. https://doi.org/10.1016/j.enggeo.2016.08.011.

Yoo, C. (2001), "Laboratory investigation of bearing capacity behavior of strip footing on geogrid-reinforced sand slope", *Geotext. Geomembranes*, **19**(5), 279-298. https://doi.org/10.1016/S0266-1144(01)00009-7.

Zhang, X. and Zhou, X. (2018), "Analysis of the numerical stability of soil slope using virtual-bond general particle dynamics", *Eng. Geol.*, **243**, 101-110. https://doi.org/10.1016/j.enggeo.2018.06.018.

Zhu, F., Clark, J.I. and Phillips, R. (2001), "Scale effect of strip and circular footings resting on dense sand", *J. Geotech. Geoenviron. Eng.*, **127**(7), 613-621. https://doi.org/10.1061/(ASCE)1090-0241(2001)127:7(613).

IC